

# Analysis of Post-Wall Waveguides and Circuits Using a Model of Two-Dimensional Photonic Crystals

Vakhtang Jandieri<sup>1, \*</sup>, Hiroshi Maeda<sup>2</sup>, Kiyotoshi Yasumoto<sup>2</sup>, and Daniel Erni<sup>1</sup>

**Abstract**—A semi-analytical method to analyze post-wall waveguides and circuits based on the model of two-dimensional photonic crystals formed by layered periodic arrays of circular cylinders is presented. The propagation constant of the fundamental TE mode, the attenuation constant due to the leakage loss and the effective width of an equivalent rectangular waveguide are calculated. Using the concept of the effective width, the original structure is replaced by an equivalent rectangular structure. When additional metallic posts are loaded in the rectangular waveguide, functional post-wall waveguide-based passive circuits are formed. The  $S$ -parameters of the post-wall circuits, which act as bandpass filters, are calculated using the image theory combined with the lattice sums technique.

## 1. INTRODUCTION

The post-wall waveguide or substrate integrated waveguide (SIW) has received a growing attention because of their promising applications to planar circuit components operating in the microwave and millimeter wave frequency range [1–5]. The post-wall waveguide is formed by periodically distributed — usually metallic — posts or the posts having a high dielectric permittivity. It allows the “planarization” of non-planar structures such as conventional rectangular and dielectric waveguides, and they can be integrated completely together with planar structures onto the same planar substrate with the same processing or fabrication techniques. The post-wall circuits are designed by inserting additional metallic or dielectric posts in the post-wall waveguide. The modal properties and performances of post-wall waveguides and circuits have been extensively investigated [also in the framework of SIWs] using various analytical or numerical techniques [1–9].

The electromagnetic field of the post-wall waveguide is confined in the lateral direction by periodic arrays of metallic posts placed on both sides of the guiding channel. The height of the waveguide bounded by two metallic plates is much smaller than the wavelength. The electromagnetic field does not change in the vertical direction, and  $TE_{m0}$ -like modes are supported in the waveguide. This kind of periodic waveguide is quite similar to a two-dimensional photonic crystal waveguide formed by parallel circular cylinders infinitely long extended along the vertical direction (no field variations along vertical direction). In the manuscript, we present a novel semi-analytical approach for analyzing such post-wall waveguides and circuits based on the model [10–14] of two-dimensional photonic crystals. The generalized reflection matrix is used to derive the dispersion equation for  $TE_{m0}$  modes. Solving the dispersion equation based on a perturbation analysis, the attenuation constant due to the leakage loss and the effective width of the equivalent rectangular waveguide are calculated. To validate the present analysis, numerical examples for the post-wall waveguides and post-wall waveguide-based passive circuits, which act as bandpass filters, are demonstrated and compared with those reported in [5–9].

---

Received 23 January 2017, Accepted 18 April 2017, Scheduled 27 April 2017

\* Corresponding author: Vakhtang Jandieri (vakhtang.jandieri@uni-due.de).

<sup>1</sup> General and Theoretical Electrical Engineering (ATE), Faculty of Engineering, University of Duisburg-Essen, and CENIDE — Center for Nanointegration Duisburg-Essen, D-47048 Duisburg, Germany. <sup>2</sup> Department of Information and Communication Engineering, Fukuoka Institute of Technology, Fukuoka 811-0295, Japan.

The scattering characteristics of the post-wall circuits are rigorously analyzed based on the lattice sums technique combined with the generalized reflection matrix method and the image theory. Perfect agreement is observed between the  $S$ -parameters over a wide frequency range.

## 2. FORMULATION OF THE PROBLEM

The post-wall waveguide, as illustrated in Fig. 1, is composed of periodic arrays of conducting circular posts (forming a planar lattice) embedded in a dielectric substrate that connect two parallel conducting plates. Fig. 1 shows the post-wall waveguide structure formed by  $N$ -layered square lattice. The electromagnetic fields are uniform in the  $y$ -direction ( $\partial/\partial y = 0$ ), and the dominant mode  $TE_{10}$  is excited. This periodic waveguide is similar to a two-dimensional photonic crystal waveguide formed by parallel circular rods, which are infinitely extended in the  $y$  direction. The photonic crystal waveguide model is schematically depicted in Fig. 2.

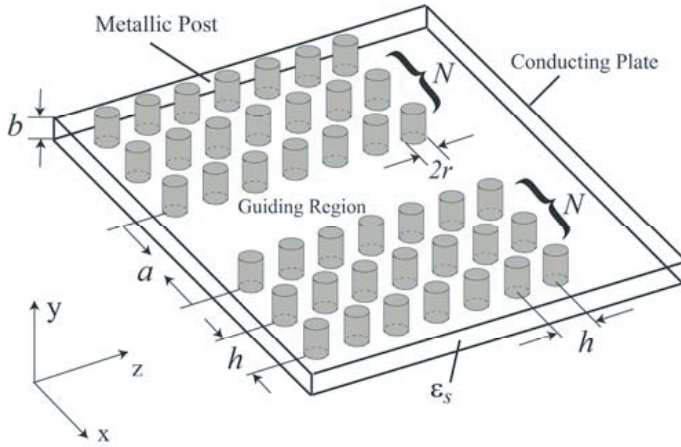


**Figure 1.** Schematic of a post-wall waveguide bounded by  $N$ -layered post-walls in both sides.

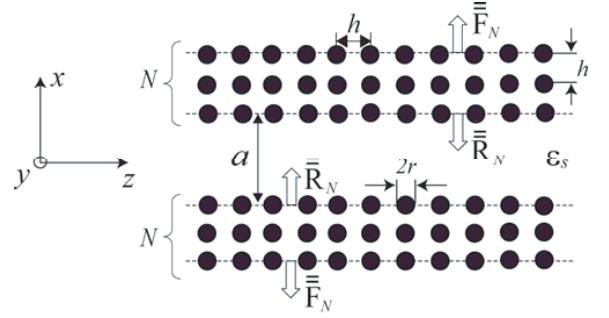


**Figure 2.** Transversal view of a two-dimensional photonic crystal waveguide to model  $N$ -layered post-wall waveguides.

Let us consider TE modes consisting of  $(E_y, H_x, H_z)$  fields. If we assume a longitudinal field variation of  $e^{i\beta z}$ , the two-dimensional guided wave propagating along the guiding region  $|x| \leq a/2$  is expressed as follows:

$$E_y(x, z) = \mathbf{U}^+(x, z) \cdot c^+ + \mathbf{U}^-(x, z) \cdot c^- \quad (1)$$

with

$$\mathbf{U}^\pm(x, z) = \{\exp[(i\kappa_\ell(x \mp a/2))] \exp(i\beta_\ell z) \delta_{\ell m}\} \quad (2)$$

$$c^\pm = [c_\ell^\pm] \quad (\ell = 0, \pm 1, \pm 2, \dots) \quad (3)$$

where  $\beta_\ell = \beta + 2\ell\pi/h$ ,  $\kappa_\ell = \sqrt{k_s^2 - \beta_\ell^2}$ ,  $k_s = \omega\sqrt{\varepsilon_s\mu_0}$ ,  $\varepsilon_s$  is the permittivity of the dielectric substrate,  $\beta$  the propagation constant, and  $c^\pm$  are the column vectors whose elements  $c_\ell^+$  and  $c_\ell^-$  represent the amplitudes of the transversally up-going and down-going  $\ell$ -th Floquet modes. The amplitude vectors  $c^\pm$  satisfy the following relations:

$$c^\pm = \mathbf{W}(\omega, \beta) \bar{\mathbf{R}}^N(\omega, \beta) \cdot c^\mp \quad (4)$$

with

$$\mathbf{W}(\omega, \beta) = [\exp(i\kappa_\ell a) \delta_{\ell m}] \quad (5)$$

where  $\mathbf{W}(\omega, \beta)$  describes the phase shift of the modes along  $x$ -direction, and  $\bar{\mathbf{R}}^N(\omega, \beta)$  denotes the generalized reflection matrix of the confining  $N$ -layered periodic arrays of circular rods, whose  $(\ell, m)$

element connects the reflected  $\ell$ -th Floquet mode to the incident  $m$ -th Floquet mode. If the lattice constants, radii of circular rods, permittivity of dielectric substrate, and number of layers  $N$  of post arrays are specified for a corresponding post-wall waveguide, the generalized reflection matrix  $\bar{\bar{\mathbf{R}}}^N(\omega, \beta)$  and transmission matrix  $\bar{\bar{\mathbf{F}}}^N(\omega, \beta)$  can be calculated [10, 11] using the  $T$ -matrix of the single circular rod together with the lattice sums. From Eq. (4), we get the transcendental equation to determine the mode propagation constant  $\beta$  as follows:

$$\det \left[ \mathbf{I} \mp \mathbf{W}(\omega, \beta) \bar{\bar{\mathbf{R}}}^N(\omega, \beta) \right] = 0 \quad (6)$$

where  $\mathbf{I}$  is the unit matrix, and the signs  $\mp$  stand for *even*( $-$ ) and *odd*( $+$ ) modes, respectively.

If only the fundamental Floquet mode with  $\ell = 0$  is propagating and all other diffraction orders are evanescent in the transverse direction, we can apply the so-called long wavelength approximation to Eq. (6). In this case, Eq. (6) is reduced to the following expression:

$$1 \mp \exp(i\kappa_0 a) \bar{\bar{R}}_{00}^N(\omega, \beta) = 0. \quad (7)$$

where  $\bar{\bar{R}}_{00}^N(\beta, \omega)$  denotes the  $(0, 0)$  element of  $\bar{\bar{\mathbf{R}}}^N(\omega, \beta)$ . As will be shown later, the reduced dispersion Equation (7) gives an excellent approximation to the full matrix Equation (6). The condition for the guided wave to be bounded by the layered post arrays shown in Fig. 2 is that all of the eigenvalues  $\lambda_k$  ( $k = 1, 2, 3, \dots$ ) of the transfer matrix over the unit cell in the  $y$  direction satisfy the relation  $|\lambda_k| < 1$  for the operating frequency range [10, 11]. This condition is always fulfilled when the operating frequency is located in the stopband of Bragg reflection in the transverse direction. Note that when the cylinders are composed of dielectrics, an enough number of layers of the periodic arrays is required to achieve the confinement of the wave field inside the guiding layer.

### 3. EQUIVALENT RECTANGULAR WAVEGUIDE

It is known [6] that when the transversal leakage of electromagnetic field through the gaps between the posts is sufficiently small, the post-wall waveguide modes practically coincide with the  $TE_{m0}$  modes of an equivalent rectangular waveguide with an effective width  $a_e = a + \Delta a$ . Let us now calculate the effective width  $a_e$  using the reduced dispersion Equation (7) for the *even* mode. If the leakage is small enough, the imaginary part of  $\beta$  due to the leakage loss can be regarded as a small perturbation. Such a treatment is allowed when  $\bar{\bar{R}}_{00}^N(\omega, \beta)$  satisfies the following condition:

$$\left| \bar{\bar{R}}_{00}^N(\beta, \omega) \right| \approx 1. \quad (8)$$

In this case, Eq. (7) yields real  $\beta(\omega)$  and  $\kappa_0(\omega)$  as unperturbed solutions. For the specified values of  $\beta(\omega)$  and  $\kappa_0(\omega)$ , the width  $a$  of the original post-wall waveguide is changed to  $a_e = a + \Delta a$  so as to satisfy the relation:

$$\exp[-i\kappa_0(\omega)(a + \Delta a)] = -1. \quad (9)$$

Equation (9) means that the boundary condition for the perfect conductor is satisfied at  $x = \pm a_e/2$ . From Eq. (9) we have:

$$a_e = \pi/\kappa_0(\omega). \quad (10)$$

Although  $a_e$  slightly changes when  $\omega$  varies, it may be practically regarded to be almost constant within the same degree of approximation as in Eq. (8). Using the equivalent rectangular waveguide model, a very simple expression for the propagation constant  $\beta_m(\omega)$  of the even  $TE_{m0}$  mode is retrieved and given below:

$$\beta_m(\omega) = \sqrt{k_s^2 - [(2m - 1)\pi/a_e]^2} \quad (m = 1, 2, 3, \dots). \quad (11)$$

### 4. LEAKAGE LOSS AND ATTENUATION CONSTANT

In this section, we describe two approaches to calculate the attenuation constant due to leakage loss in post-wall waveguide. If  $|\bar{\bar{R}}_{00}^N(\beta, \omega)| = 1$ , the real values of the propagation constant  $\beta_0$  can be obtained

by numerically solving Eq. (7). The decrement of  $|\bar{R}_{00}^N(\beta, \omega)|$  from unity is caused by the transverse leakage of the guided field. Let us introduce a small attenuation constant  $\alpha$  of the guided wave due to the leakage and express the propagation constant  $\beta$  as:

$$\beta = \beta_0 + i\alpha \quad (\alpha \ll \beta_0). \quad (12)$$

Under this condition, Eq. (7) for the fundamental mode is approximated as follows:

$$\exp(-i\kappa_0 a) \exp\left(-\frac{\beta_0 a}{\kappa_0} \alpha\right) = \bar{R}_{00}^N(\beta_0, \omega) \quad (13)$$

where  $\kappa_0 = \sqrt{k_s^2 - \beta_0^2}$ . Note that in Eq. (13) we have ignored the small perturbation to the real part of  $\beta$  due to the deviation of  $|\bar{R}_{00}^N(\beta_0, \omega)|$  from unity. As will be shown later, this approximation is well justified by the fact that the difference between the real part of the propagation constants  $\beta$  calculated for  $N = 1$  and for  $N = \infty$  without leakage losses is negligibly small. From Eq. (13), the attenuation constant  $\alpha$  due to the leakage is given as follows:

$$\alpha = -\frac{\kappa_0}{\beta_0 a} \ln \left| \bar{R}_{00}^N(\beta_0, \omega) \right|. \quad (14)$$

The attenuation constant  $\alpha$  can also be calculated using a perturbation analysis taking into account the principle of power conservation. Due to leakage the guided waves carrying a total power  $P_z = \int_0^{a/2} \text{Re}\{-E_y H_x^*\} dx$  will attenuate as a function of  $z$  (\* denotes the complex conjugate). Assuming that the amplitudes of the fields decay exponentially with an attenuation constant  $\alpha$ , and the carrier power  $P_z$  will show an exponential decay according to  $P_z \sim e^{-2\alpha z}$ . By the power conservation principle, the decrease of  $P_z$  along  $z$  direction should be equal to the transversal power dissipation per unit length  $\langle S_x \rangle = \frac{1}{2h} \int_0^h \text{Re}\{E_y H_z^*\} dz$ . As a result, taking into account the orthogonality of the Floquet modes, the attenuation constant  $\alpha$  can be now expressed in the following form:

$$\alpha = \frac{\langle S_x \rangle}{P_z} = 0.5\kappa_0 \left| \bar{F}_{00}^N \right|^2 \times \left[ \frac{\beta}{\kappa_0} [\sin(\kappa_0 a) + \kappa_0 a] + \sum_{\substack{\ell=-M \\ (\ell \neq 0)}}^M \frac{\beta_\ell}{\gamma_\ell} e^{-\gamma_\ell a} [\sinh(\gamma_\ell a) + \gamma_\ell a] \left| \bar{R}_{\ell 0}^N \right|^2 \right]^{-1} \quad (15)$$

where  $\gamma_\ell = \sqrt{\beta_\ell^2 - k_s^2}$  denotes a propagation constant of the evanescent modes and  $M$  stands for the truncation number of the modes. Equation (15) takes into account all interactions between the Floquet modes.

## 5. NUMERICAL RESULTS AND DISCUSSIONS

In order to confirm the validity of the long wavelength approximation to the dispersion equation, firstly we have calculated the propagation constant  $\beta$  of the fundamental  $TE_{10}$  mode by using the full matrix Equation (6) and the reduced Equation (7), respectively, and compared both results. We assumed that the conductor loss in post-walls and the dielectric loss in the substrate are negligible. The first example encompasses a post-wall structure with  $\varepsilon_s/\varepsilon_0 = 2.33$ ,  $h = 2.0$  mm,  $r = 0.4$  mm and  $a = 7.2$  mm [5, 6, 8]. Since  $h/r = 5.0$  and  $h/a = 0.278$ , the gap width between two nearby posts is relatively small. The normalized propagation constants calculated from Eqs. (6) and (7) for different numbers  $N$  of layers of the post-walls are compared in Table 1. Note that the value of  $\beta h/2\pi$  calculated for Eq. (6) at  $N = \infty$  gives a rigorous value of the normalized propagation constant because the guided field is completely bounded for  $N = \infty$  (note that from the practical point of view, it is enough to have about  $N = 5$  layers along the  $x$ -axis in order to get the strong confinement of the modes in the guiding region). From Table 1, we can see that although the propagation constant calculated by Eq. (6) changes as the number  $N$  of post-walls increases, the difference between those for  $N = 1, 2, 3$  and  $N = \infty$  is vanishingly small. It is worth mentioning that the propagation constant calculated by the reduced dispersion Equation (7) for  $N = 1$  is in very close agreement with the rigorous values obtained for  $N = \infty$  with an accuracy of four digits. In particular, the relative error for  $N = 1$  is: 0.2315% at  $f = 15$  GHz, 0.0212% at

**Table 1.** Normalized propagation constants  $\beta h/2\pi$  of the fundamental  $TE_{10}$  mode for the  $N$ -layered post-wall waveguide with  $\epsilon_s/\epsilon_0 = 2.33$ ,  $h = 2.0$  mm,  $r = 0.4$  mm and  $a = 7.2$  mm. The propagation constants obtained from the rigorous transcendental Equation (6) and the reduced dispersion Equation (7) are compared.

	$\beta h/2\pi$				
	Eq. (6)				Eq. (7)
$f$ [GHz]	$N = 1$	$N = 2$	$N = 3$	$N = \infty$	$N = 1$
15.0	0.04330	0.04320	0.04320	0.04320	0.04330
20.0	0.14143	0.14140	0.14140	0.14140	0.14143
25.0	0.20811	0.20808	0.20808	0.20808	0.20829
30.0	0.26812	0.26810	0.26810	0.26810	0.26811

**Table 2.** Normalized propagation constants  $\beta h/2\pi$  of the higher order  $TE_{20}$  and  $TE_{30}$  modes calculated by using Eq. (11) for the 1-layer post-wall waveguide with  $\epsilon_s/\epsilon_0 = 2.33$ ,  $h = 2.0$  mm,  $r = 0.4$  mm and  $a = 7.2$  mm.

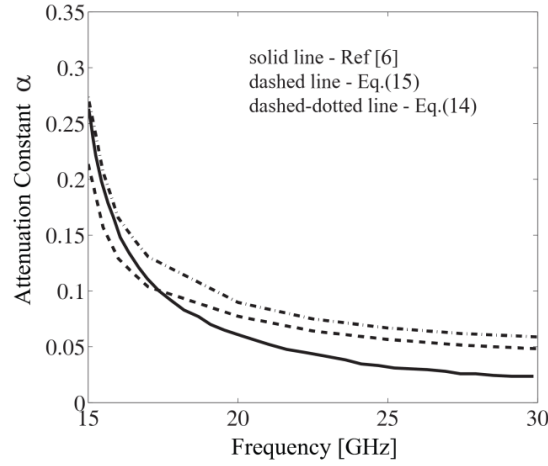
		$N = 1$		
$TE_{m0}$	$f$ [GHz]	$\beta h/2\pi$ Eq. (7)	$\kappa_0 h$	$\beta h/2\pi$ Eq. (11)
$TE_{20}$ (odd mode)	30.0	0.08880	0.9173	0.08902
	35.0	0.20438	0.9155	0.20477
	40.0	0.28460	0.9134	0.28488
	45.0	0.35421	0.9104	0.35457
$TE_{30}$ (even mode)	45.0	0.14021	0.9104	0.14404
	50.0	0.26480	0.9007	0.27192
	55.0	0.35618	0.8998	0.35870

$f = 20$  GHz, 0.0144% at  $f = 25$  GHz and 0.0075% at  $f = 30$  GHz. It follows that if the gap between the nearby posts is small, the leakage of the guided wave through the gap becomes negligibly small and hence the guiding condition for  $TE_{10}$  mode is well fulfilled even for  $N = 1$ .

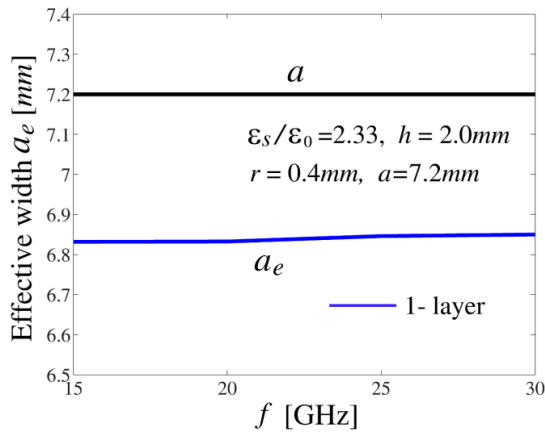
Table 2 shows the comparison of the normalized propagation constants  $\beta h/2\pi$  of the calculated higher-order  $TE_{20}$  and  $TE_{30}$  modes based on Eqs. (7) and (11). Other geometrical parameters are the same as those in Table 1. The cutoff frequencies of the  $TE_{20}$  odd mode and the  $TE_{30}$  even mode are 28.77 GHz and 43.16 GHz, respectively. A very good agreement is observed over the wide frequency range.

Figure 3 demonstrates the dependence of the attenuation constant  $\alpha$  versus the frequency in the range of 15 GHz–30 GHz. The dashed-dotted line and dashed line represent the attenuation constants based on Eqs. (14) and (15), respectively, which are then compared to the values shown in [6]. A good agreement is observed in the whole frequency range; however, it should be noted that the given attenuation constants  $\alpha$  are slightly larger than those reported in [5, 6, 8]. Additionally, it should be mentioned that the data for the calculated attenuation constant based on Eq. (15) is closer to the reference data. This could be explained by the fact that Eq. (15) is a more general expression, since it takes into account all interactions between the Floquet modes.

Figure 4 demonstrates the values of the effective width  $a_e$  of the equivalent rectangular waveguide calculated based on Eq. (10) for post-wall waveguide with  $\epsilon_s/\epsilon_0 = 2.33$ ,  $h = 2.0$  mm,  $r = 0.4$  mm,  $a = 7.2$  mm, and  $N = 1$ . We can see that the effective width  $a_e$  is slightly smaller than the physical distance  $a$  between two post-walls and increases in proportion to the operating frequency  $f$ . Although the effective width  $a_e$  slightly changes depending on the frequency, its variation is very small and less than 0.3% in the range of 15 GHz–30 GHz. If we define the effective width  $a_e$  as a constant structural



**Figure 3.** Attenuation constant  $\alpha$  calculated using (14) and (15) plotted by the dashed-dotted line and dashed line, respectively, is compared with Ref. [6] represented by the solid line.



**Figure 4.** Effective width  $a_e$  of the equivalent rectangular waveguide calculated using (10) versus frequency for  $\varepsilon_s/\varepsilon_0 = 2.33$ ,  $h = 2.0$  mm,  $r = 0.4$  mm,  $a = 7.2$  mm, and  $N = 1$ .

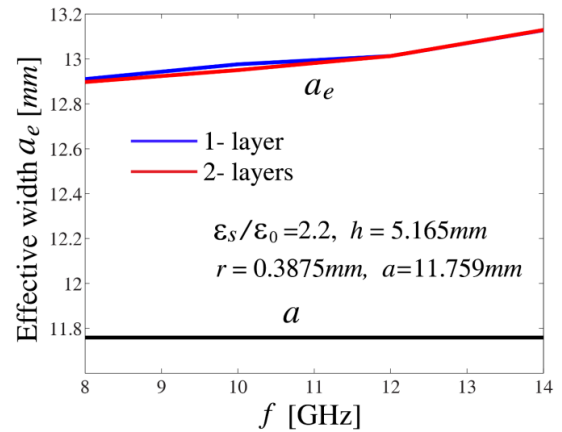


**Figure 5.** Effective width  $a_e$  of the equivalent rectangular waveguide calculated using (10) versus frequency for  $\varepsilon_s/\varepsilon_0 = 2.2$ ,  $h = 5.165$  mm,  $r = 0.3875$  mm,  $a = 11.759$  mm, and  $N = 1$  (blue line) and  $N = 2$  (red line).

parameter, we can employ a value for  $a_e$  that is averaged over the operating frequency range. The post-wall waveguide filters will be analyzed later in this section by using the averaged value of  $a_e$  as a fixed effective width over the operating bandwidth.

The second example includes a structure with  $\varepsilon_s/\varepsilon_0 = 2.2$ ,  $h = 5.165$  mm,  $r = 0.3875$  mm, and  $a = 11.759$  mm after [6]. Since  $h/r = 13.329$  and  $h/a = 0.439$ , the gap width is much larger than that of the first example. Table 3 shows the comparison of the normalized propagation constants calculated from Eqs. (6) and (7) for different numbers of layers  $N$  of the post-walls. We can see that the propagation constant calculated by the reduced dispersion Equation (7) for  $N = 1$  is not in excellent agreement with that calculated by Equation (6) for  $N = \infty$ . Particularly, the relative error for  $N=1$  is: 4.3806% at  $f = 8$  GHz, 0.2625% at  $f = 10$  GHz, 0.1753% at  $f = 12$  GHz and 0.0837% at  $f = 14$  GHz. Since the gap width (a distance between the nearest rods) is relatively large, it is rather difficult to confine the guided field by a single-layered post-wall. The leakage through the periodic gaps will give a significant rise to the attenuation of guided waves and thus affect the propagation constant  $\beta$ . Fig. 5 illustrates that the

**Table 3.** Normalized propagation constants  $\beta h/2\pi$  of the fundamental  $TE_{10}$  mode for the  $N$ -layered post-wall waveguide with  $\epsilon_s/\epsilon_0 = 2.2$ ,  $h = 5.165$  mm,  $r = 0.3875$  mm, and  $a = 11.759$  mm. The propagation constants obtained from the rigorous transcendental Equation (6) and the reduced dispersion Equation (7) are compared.

$f$ [GHz]	$\beta h/2\pi$				
	Eq. (6)				Eq. (7)
	$N = 1$	$N = 2$	$N = 3$	$N = \infty$	$N = 1$
8.0	0.04152	0.04056	0.04056	0.04060	0.04246
10.0	0.15980	0.15956	0.15956	0.15956	0.15998
12.0	0.23368	0.23352	0.23352	0.23353	0.23394
14.0	0.29844	0.29836	0.29836	0.29853	0.29878

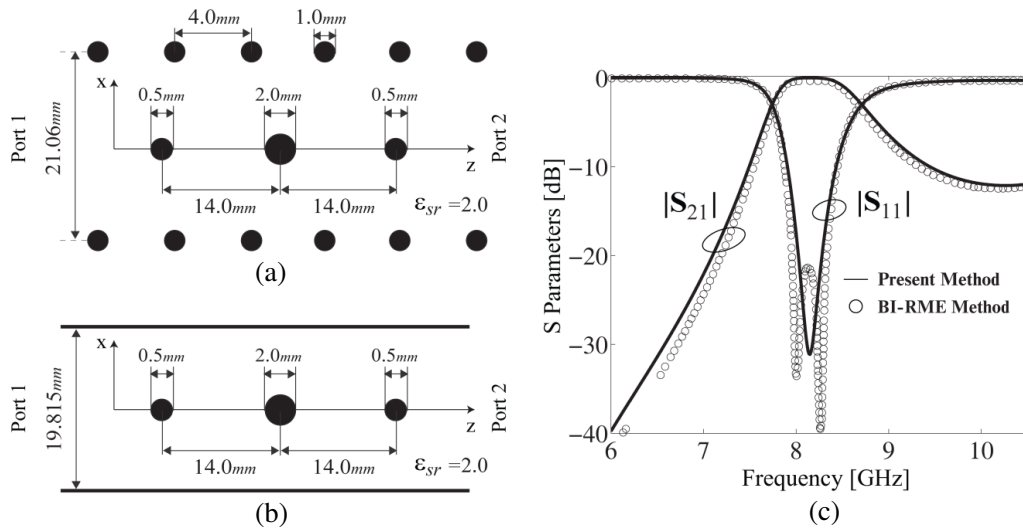


**Figure 6.** Bandpass filter with three circular posts of conductor: (a) Original post-wall waveguide structure; (b) Equivalent rectangular waveguide structure, and (c)  $S$ -parameters of the circuit (a).

effective width  $a_e$  does not change significantly even if the number of post-wall layers is increased. It is worth emphasizing that for the present structure with a wider gap as  $h/r = 13.329$ , the effective width  $a_e$  becomes larger than the physical width  $a$  of the post-wall waveguide. As the gap width increases, the rate of leakage of guided wave increases. This situation is quite different from that of a narrow gap case discussed in the first example.

Finally, we shall analyze two post-wall waveguide bandpass filters by using the method of images (Appendix A). The interested readers may refer to [15]. When a post-wall waveguide structure is specified, firstly we calculate its effective width  $a_e$  by using Eq. (10) and define an equivalent rectangular waveguide. We calculated the scattering parameters in the rectangular waveguide by using the image theory and the two-dimensional photonic-crystal model. Two numerical examples for ultra-compact bandpass filter by using the boundary integral-resonant mode expansion (BI-RME) method [7] and a hybrid method [9] are shown in Figs. 6 and 7. The  $S$ -parameters calculated by the proposed method are compared with those in [7, 9]. We observe that all of the  $S$ -parameters obtained by the present method are in excellent agreement with those reported in [7, 9]. For the structure shown in Fig. 6(a), the material loss was ignored in our analysis, but a conductor loss of  $\sigma_c = 4 \times 10^7$  S/m and a dielectric loss of  $\sigma_d = 0.001$  S/m were considered in [7]. The small difference in the  $S$ -parameters observed in Fig. 6(c) is due to slightly different assumptions of the material loss.

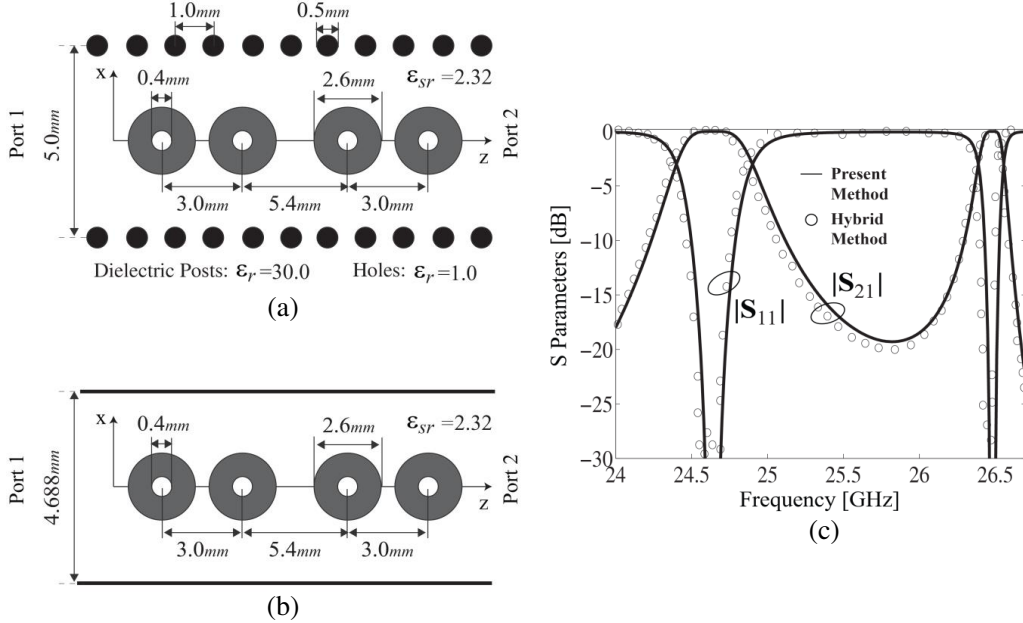


**Figure 7.** Dual-band bandpass filter with four concentric circular posts of dielectric with air-hole: (a) Original post-wall waveguide structure; (b) Equivalent rectangular waveguide structure, and (c)  $S$ -parameters of the circuit (a).

## 6. CONCLUSION

In the manuscript, we have reported a novel semi-analytical approach for analyzing post-wall waveguides and circuits based on the model of two-dimensional photonic crystals. The generalized reflection matrix is used to derive the dispersion equation for  $TE_{m0}$  modes. Solving this dispersion equation based on a perturbation analysis, the attenuation constant (due to the leakage loss) and the effective width of the equivalent rectangular waveguide are calculated. To validate the proposed formalism, numerical examples for post-wall waveguides and post-wall waveguide-based passive circuit, such as bandpass filter, are presented and compared to other references yielding a perfect agreement between the  $S$ -parameters over a wide frequency range. It is important to mention that the proposed semi-analytical formulation is not time-consuming, which could be considered as a major advantage of the proposed formulation. The desktop CPU runtime on the 3.6 GHz Intel Core i7 with 8 GB RAM per one frequency is around 0.2 second. The authors believe that the proposed method is a very apt tool for designing advanced multi-functional, ultra-compact submillimeter passive circuit devices. It is expected to give an insight into the physics underlying the proper guiding mechanism in such periodic waveguide structures and/or bandgap (meta) materials.

## ACKNOWLEDGMENT

V. Jandieri acknowledges financial support from the Alexander von Humboldt Foundation. The work is supported by Shota Rustaveli National Science Foundation (SRNSF) (Grant No. 216662 and Grant No. FR/25/6-100/14) The work is also supported by JSPS KAKENHI (Grant No. 24560430). D. Erni acknowledges the support from the DFG SFB/TRR 196 MARIE.

## APPENDIX A.

Post-wall waveguide filters are designed by carefully inserting multiple circular full posts into the guiding region as shown in Fig. A1(a). If we employ the effective width  $a_e$  for the post-wall waveguide discussed



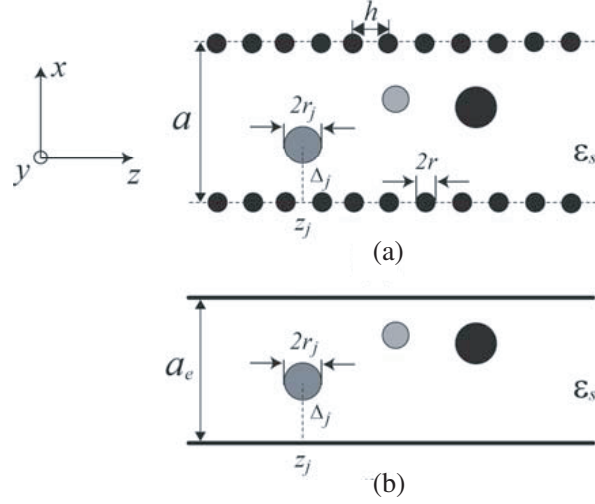


**Figure A1.** Top view of circular posts inserted into (a) a post-wall waveguide and into (b) equivalent rectangular waveguide with the effective width  $a_e$ .

in Section 3, the original structure is replaced by the equivalent rectangular waveguide structure shown in Fig. A1(b). In this section, we briefly present an accurate and rigorous approach for analyzing the scattering properties of the vertical posts and relevant electromagnetic bandgap structures in such a rectangular waveguide. The interested readers may be referred to [15].

Let us consider the  $i$ -th post with radius  $r_j$  whose center is located at  $(\Delta_j, z_j)$  within the equivalent rectangular waveguide. The excitation is assumed to be in  $TE_{m0}$  mode. The excitation in the forward direction is expanded into the cylindrical waves as following:

$$E_{y,m}^i = a_m^+ \sin(\kappa_m x) \exp(i\beta_m z) = \Phi_1^T \cdot \mathbf{p}_m^+ \cdot a_m^+ \quad (\text{A1})$$

with

$$\Phi_1 = [J_n(k_s \rho_0^+) \exp(in\phi_0^+)] \quad (\text{A2})$$

$$\mathbf{p}_m^+ = [p_{mn}^+], \quad p_{mn}^+ = \left[ \frac{1}{2} (-i)^{n-1} \{ \exp[i(n\theta_m - \kappa_m \Delta_j)] - (-1)^n \exp[-i(n\theta_m - \kappa_m \Delta_j)] \} \right] \quad (\text{A3})$$

$$\cos \theta_m = \frac{\kappa_m}{k_s}, \quad \rho_0^+ = \sqrt{(x - \Delta_j)^2 + (z - z_j)^2}, \quad \cos \phi_0^+ = \frac{x - \Delta_j}{\rho_0^+} \quad (\text{A4})$$

where  $\kappa_m = \frac{m\pi}{a}$  ( $m = 1, 2, \dots$ ),  $\beta_m$  is the propagation constant of the  $m$ -th mode,  $a_m^+$  labels the amplitude of the incident field,  $J_n$  the  $n$ -th order Bessel function, and  $(\rho_0^+, \phi_0^+)$  the polar coordinates with the origin at the center of the post. Taking into account an infinite number of mirror images of the post with respect to the side walls, the scattered field is expressed as:

$$E_y^s = \sum_{\ell=-\infty}^{\infty} \sum_{n=-\infty}^{\infty} X_n H_n^{(1)}(k_s \rho_\ell^+) \exp(in\phi_\ell^+) - \sum_{\ell=-\infty}^{\infty} \sum_{n=-\infty}^{\infty} (-1)^n X_n H_n^{(1)}(k_s \rho_\ell^-) \exp(-in\phi_\ell^+) \quad (\text{A5})$$

with

$$\rho_\ell^\pm = \sqrt{(x_\ell \mp \Delta_j)^2 + (z - z_j)^2}, \quad \cos \phi_\ell^\pm = \frac{x_\ell \mp \Delta_j}{\rho_\ell^\pm} \quad (\text{A6})$$

where  $x_\ell = x - 2a\ell$ ,  $H_n^{(1)}$  is the  $n$ -th order Hankel function of the first kind.  $X_n$  are unknown amplitudes of the scattered multipole fields, and  $(\rho_\ell^\pm, \phi_\ell^\pm)$  are the local polar coordinates with the origins at  $(2a\ell \pm \Delta_j, z_j)$ . The array has a period of  $2a$  and contains two cylinders within its unit cell. Thus, the problem is reduced to that of a two-dimensional scattering problem from the layered periodic arrays of parallel circular cylinders. Following the same calculation procedure as shown in [15], first,

the unknown scattering amplitudes  $X_n$  are expressed in a closed form through the lattice sums, the translation matrices of cylindrical waves and the  $T$ -matrix of the circular cylinder in isolation. Next, using a Fourier integral representation of the Hankel functions, the multipole fields are transformed into a series of space harmonics of plane waves, and the reflection and transmission matrices of the posts for the incident  $TE_{m0}$  mode are derived. Finally, a recurrence formula is applied to obtain the generalized reflection and transmission matrices characterizing the layered structure.

## REFERENCES

1. Hirokawa, J. and M. Ando, "Single-layer feed waveguide consisting of posts for plane TEM wave Excitation in parallel plates," *IEEE Trans. Antennas Propagat.*, Vol. 46, No. 5, 625–630, 1998.
2. Uchiyama, H., T. Takenoshita, and M. Fujii, "Development of a "laminated waveguide"," *IEEE Trans. Microwave Theory Tech.*, Vol. 46, No. 12, 2438–2443, 1998.
3. Entesari, K., A. P. Saghati, V. Sekar, and M. Armendariz, "Tunable SIW structures," *IEEE Microwave Magazine*, 34–54, June 2015.
4. Yan, L., W. Hong, K. Wu, and T. J. Cui, "Investigations on the propagation characteristics of the substrate integrated waveguide based on the method of lines," *IEE Proc. — Microw. Antennas Propag.*, Vol. 152, No. 1, 35–42, 2005.
5. Xu, F. and K. Wu, "Guided-wave and leakage characteristics of substrate integrated waveguide," *IEEE Trans. Microwave Theory Tech.*, Vol. 53, No. 1, 66–73, 2005.
6. Deslandes, D. and K. Wu, "Accurate modeling, wave mechanisms, and design considerations of a substrate integrated waveguide," *IEEE Trans. Microwave Theory Tech.*, Vol. 54, No. 6, 2516–2526, 2006.
7. Bozzi, M., F. Xu, L. Perregri, and K. Wu, "Circuit modeling and physical interpretation of substrate integrated waveguide structures for millimeter-wave applications," *Int. J. Microwave Opt. Technol.*, Vol. 3, No. 3, 329–338, 2008.
8. Kishihara, M., I. Ohta, K. Okubo, and J. Yamakita, "Analysis of post-wall waveguide based on  $H$ -plane planar circuit approach," *IEICE Trans. Electronics*, Vol. E92-C, No. 1, 63–71, 2009.
9. Wu, X. H. and A. A. Kishk, "Hybrid of method of moments and cylindrical eigenfunction expansion to study substrate integrated waveguide circuits," *IEEE Trans. Microwave Theory Tech.*, Vol. 56, No. 10, 2270–2276, 2008.
10. Yasumoto, K., H. Toyama, and T. Kushta, "Accurate analysis of two-dimensional electromagnetic scattering from multilayered periodic arrays of circular cylinders using lattice sums technique," *IEEE Trans. Antennas Propagat.*, Vol. 52, No. 10, 2603–2611, 2004.
11. Yasumoto, K., *Electromagnetic Theory and Applications for Photonic Crystals*, Chapter 3, CRC Press, 2005.
12. Yasumoto, K., H. Jia, and K. Sun, "Rigorous modal analysis of two-dimensional photonic crystal waveguides," *Radio Sci.*, Vol. 40, No. 6, RS6S02, 2005.
13. Jandieri, V., K. Yasumoto, and J. Pistora, "Coupled-mode analysis of contra-directional coupling between two asymmetric photonic crystals waveguides," *Journal of the Optical Society of America A*, Vol. 31, No. 3, 518–523, 2014.
14. Yasumoto, K., H. Maeda, and V. Jandieri, "Analysis of post-wall waveguides using a model of two-dimensional photonic crystal waveguides," *Proceedings of the IEEE International Conference on Signal Processing and Communication (ICSC-2015)*, 74–79, Noida, India, April 2015.
15. Yasumoto, K., N. Koike, H. Jia, and B. Gupta, "Analysis of electromagnetic bandgap based filters in a rectangular waveguide," *IEICE Trans. Electronics*, Vol. E89-C, No. 9, 1324–1329, 2006.